Three-Dimensional Solution Structure of the Calcium-Signaling Protein Apo-S100A1 As Determined by NMR[†,‡]

Richard R. Rustandi,[§] Donna M. Baldisseri,[§] Keith G. Inman,[§] Peter Nizner,[§] Shannon M. Hamilton,[§] Aimee Landar,[||] Alexander Landar,[||] Danna B. Zimmer,[||] and David J. Weber*[,§]

Department of Biochemistry and Molecular Biology, University of Maryland School of Medicine, 108 North Greene Street, Baltimore, Maryland 21201, and Department of Pharmacology, College of Medicine, University of South Alabama, MSB 3130, Mobile, Alabama 36688

Received September 24, 2001; Revised Manuscript Received November 12, 2001

ABSTRACT: S100A1, a member of the S100 protein family, is an EF-hand containing Ca^{2+}-binding protein (93 residues per subunit) with noncovalent interactions at its dimer interface. Each subunit of S100A1 has four α-helices and a small antiparallel β-sheet consistent with two helix−loop−helix calcium-binding domains [Baldiserri et al. (1999) *J. Biomol. NMR 14, 87−88*]. In this study, the three-dimensional structure of reduced apo-S100A1 was determined by NMR spectroscopy using a total of 2220 NOE distance constraints, 258 dihedral angle constraints, and 168 backbone hydrogen bond constraints derived from a series of 2D, 3D, and 4D NMR experiments. The final structure was found to be globular and compact with the four helices in each subunit aligning to form a unicornate-type four-helix bundle. Intermolecular NOE correlations were observed between residues in helices 1 and 4 from one subunit to residues in helices 1′ and 4′ of the other subunit, respectively, consistent with the antiparallel alignment of the two subunits to form a symmetric X-type four-helix bundle as found for other members of the S100 protein family. Because of the similarity of the S100A1 dimer interface to that found for S100B, it was possible to calculate a model of the S100A1/B heterodimer. This model is consistent with a number of NMR chemical shift changes observed when S100A1 is titrated into a sample of ^{15}N-labeled S100B. Helix 3 (and 3′) of S100A1 was found to have an interhelical angle of −150° with helix 4 (and 4′) in the apo state. This crossing angle is quite different (>50°) from that typically found in other EF-hand containing proteins such as apocalmodulin and apotroponin C but more similar to apo-S100B, which has an interhelical angle of −166°. As with S100B, it is likely that the second EF-hand of apo-S100A1 reorients dramatically upon the addition of Ca^{2+}, which can explain the Ca^{2+} dependence that S100A1 has for binding several of its biological targets.

S100A1[1] is a member of the S100 family of cytoplasmic and extracellular Ca^{2+}-binding proteins (*1*−*4*). These proteins were originally isolated from brain and called S100 to denote their solubility in 100% saturated ammonium sulfate. Further studies demonstrated that the S100 fraction in brain was comprised of primarily two highly homologous proteins, S100A1 and S100B (60% sequence identity). These two proteins can exist as homodimers [S100A1(αα), S100B(ββ)] or as a heterodimer (S100A1/B). Presently, the S100 family contains approximately 21 members, and they are distributed in a tissue-specific manner (*1*, *2*, *4*, *5*). The genes encoding S100A1-A14, two other S100 fusion proteins, and several epidermal differentiation genes map to human chromosome 1q21 (*6*). The remaining family members are located on different chromosomes: S100B maps to chromosome 21q22, S100P maps to chromosome 4q16, and CABL maps to chromosome Xp22. The list of diseases associated with altered expression of an S100 family member is extremely diverse and includes cancer, Alzheimer's disease, multiple sclerosis, diabetes, psoriasis, rheumatoid arthritis, pulmonary hypertension, and cardiomyopathy.

Genetic manipulation of neuronal PC12 cells has revealed three phenotypic changes that occur in S100A1-expressing cells. These include increased proliferation, decreased cytoskeletal organization, altered Ca^{2+} homeostasis, and increased susceptibility to Aβ toxicity (*7*). These phenotypic changes are mediated by S100A1 regulation of tubulin synthesis, tubulin polymerization, and ionomycin-sensitive Ca^{2+} stores. Determination of the number and identity of

[†] This work was supported by NIH Grants GM58888 (to D.J.W.) and NS30660 (to D.B.Z.) and by grants from the American Cancer Society, RPG0004001CCG (to D.J.W.), and the Pine Family Foundation (to D.B.Z.).

[‡] The coordinates for the apo-S100A1 3D structure were deposited in the Protein Data Bank (accession numbers: PDB, 1K2H; RCSB, 014477).

* Corresponding author. Phone: (410) 706-4354. Fax: (410) 706-0458. E-mail: dweber@umaryland.edu.

[§] University of Maryland School of Medicine.

[||] University of South Alabama.

[1] Abbreviations: DTT, dithiothreitol; S100A1, homodimeric S100A1(αα) with noncovalent interactions at the dimer interface; S100α, subunit of dimeric S100A1; S100β, subunit of dimeric S100B; S100B(ββ) or S100B, dimeric S100B with noncovalent interactions at the dimer interface; S100A1/B, heterodimer that has a single S100A1 α-subunit and a single S100B β-subunit held together noncovalently; rmsd, root mean square difference; NOE, nuclear Overhauser effect; NMR, nuclear magnetic resonance; HSQC, heteronuclear single-quantum coherence; TPPI, time-proportional phase incrementation; 3D, three dimensional.

10.1021/bi0118308 CCC: $22.00
Published on Web 12/21/2001

the target proteins involved in these processes is essential for understanding the physiological function of S100A1.

The biological functions of most S100 proteins depend on Ca^{2+} concentrations inside the cell. This is because all of the members of this protein family contain two helix−loop−helix Ca^{2+} ion-binding domains per subunit referred to as the *typical* and *pseudo*-EF-hand motifs. The pseudo-EF-hand has 14 rather than 12 residues and generally binds Ca^{2+} with a lower affinity (K_d > 50 μM) than the typical EF-hand (K_d < 50 μM) (*8*−*10*). Structural studies have demonstrated that Ca^{2+} ion binding induces the reorientation of helix 3 for most but not all of the family members, and the extent of this conformational change can vary (*11*). Generally, the change in the position of helix 3 exposes a hydrophobic surface that interacts with other proteins referred to as target proteins. In the case of S100A1, mutagenesis studies indicate that several hydrophobic residues in the carboxy terminus (i.e., F88, F89, and W90) are important for this Ca^{2+}-dependent target protein interaction (*12*, *13*). However, because of a lack of homology in the C-terminus and in a loop connecting the EF-hands termed the *hinge region*, the list of target proteins for each S100 family member is extensive and diverse (*2*).

The functions of S100 proteins are also affected by the different physical properties of individual family members. The affinity of family members for Ca^{2+}, Cu^{2+}, and Zn^{2+} varies considerably. S100A10 has variations in the Ca^{2+}-binding consensus sequence in both EF-hands that render it unable to bind Ca^{2+}, while S100B binds Ca^{2+}, Cu^{2+}, and Zn^{2+} with high affinity. Additional diversity is generated by the oligomerization properties of the individual family members. S100 family members, with the exception of calbindin D_{9K}, exist in a homodimeric state. Two types of S100B homodimers have been detected: a disulfide-linked dimer referred to as S100B($\beta_{S-S}\beta$) and a noncovalent dimer, S100B($\beta\beta$). The disulfide-linked dimer is critical for extracellular activities of S100B such as neurite extension and cell survival (*2*, *5*, *10*). However, on the basis of the location of cysteine residues in S100B, the structure of the disulfide-linked S100B($\beta_{S-S}\beta$) dimer must be considerably different from that of the reduced form. While other family members have extracellular functions and many contain cysteine residues, only S100A11 and S100A8 (*14*) function predominantly as a disulfide-linked dimer. For other S100 proteins, such as S100A1, S100B, S100A4, and S100A6, the intracellular form presented to target proteins is the noncovalent dimer. The dimer predominates inside the cell because of the reducing environment, the dimers' high-affinity subunit association [$^{S100B}K_D$ < 1 nM (*15*)], and the relatively high intracellular abundance of most S100 proteins (micromolar concentrations).

The diversity of biological function of this protein family is even further increased because several S100 proteins form noncovalent heterodimers with subunits from other family members. For example, the S100A8/A9 heterodimer exists in neutrophils (*16*, *17*), and S100A1/B heterodimers were isolated from neural tissue (*18*). In the case of S100A8 and S100A9, heterodimerization is Ca^{2+}-dependent. S100A1/S100A4 heterodimers (*19*, *20*) were also detected using yeast two-hybrid approaches, but without confirmation of the functionality of the various fusion proteins used in the yeast two-hybrid experiments, definitive conclusions regarding heterodimerization in these cases are still somewhat premature. Nonetheless, since it is possible that target protein binding affects the oligomerization state of these Ca^{2+}-binding proteins (*15*), it is imperative that all possible oligomerization and heterodimeric states are considered in functional studies.

Accurately defined three-dimensional (3D) structures are required to determine how specific S100 family members bind unique targets to elicit different biological effects. Recently, NMR spectroscopy and X-ray crystallography were used to solve the high-resolution 3D structures of several S100 proteins in the apo (Ca^{2+} free), holo (Ca^{2+} bound), and target protein-bound states (for review see ref *11*). As a first step in determining how S100A1 binds its target proteins, we have determined the structure of apo-S100A1 in solution using data from a series of multidimensional NMR experiments. Like many of the other S100 protein structures determined thus far, S100A1 is a homodimeric protein held together at the dimer interface by a characteristic X-type four-helix bundle. Because of the similarity between this dimer interface and that found for S100B, it was possible to calculate a model of the S100A1/B heterodimer. This apo-S100A1 structure together with the model of the S100A1/B heterodimer gives additional insights about how the tight dimer interface forms in this protein family. In addition, helix 3 in S100A1 is positioned similarly to the corresponding helix in apo-S100B. Therefore, as for S100B, a large reorientation of helix 3 is expected to occur for S100A1 when Ca^{2+} binds. This conformational change is required for S100A1 to interact with several target proteins, as is now the paradigm for several dimeric S100 proteins. A preliminary report of the assignments and the secondary structure of S100A1 have been published previously (*21*).

METHODS

NMR Sample Preparation. Isotopically enriched [^{13}C]-glucose (>99%) and $^{15}NH_4Cl$ (>99%) were purchased from Cambridge Isotope Laboratories (Woburn, MA). As previously described (*12*), wild-type recombinant S100A1 protein was overexpressed in *Escherichia coli* (HMS174(DE3) strain) transformed with an expression plasmid (pET-11b; Novagen Inc.) containing the gene for rat S100A1. Unlabeled, ^{15}N-labeled, and ^{13}C,^{15}N-labeled S100A1 were purified under reducing conditions using a modification of the procedure described by Landar et al. (*12*). After dialysis, the 60% ammonium sulfate supernatant fraction was chromatographed on DEAE-Sepharose, and the S100A1 fractions were eluted with 0.3 M NaCl. The S100A1-containing fractions from DEAE chromatography were then applied to phenyl-Sepharose (Pharmacia, Piscataway, NJ) in the presence of 10 mM $CaCl_2$, and pure S100A1 (>99%) was eluted with 10 mM EDTA. The identity and purity of S100A1 were confirmed by amino acid analysis and electrospray mass spectrometry. The samples used for NMR spectroscopy contained ^{13}C,^{15}N-labeled or ^{15}N-labeled S100A1 (2.4−3.2 mM) or ^{15}N-labeled rat S100B (3 mM; for the heterodimer titration), d_{11}-Tris (12−15 mM), EGTA (1−2 mM), NaN_3 (0.3 mM), NaCl (15−18 mM), and D_2O (5%), pH 6.4. All solutions used in the NMR samples were pretreated with Chelex to remove trace metals.

NMR Spectroscopy. NMR spectra were collected at 37 °C with a Bruker DMX600 NMR spectrometer (600.13 MHz

for protons) equipped with four frequency channels and a triple resonance three-axis gradient probe (Table 1s, Supporting Information). Unless otherwise stated, multidimensional NMR data were collected in the indirect dimensions using States−TPPI phase cycling (*22*) using a 1 s relaxation delay. Sequential backbone and side chain assignments of S100A1 were obtained using standard heteronuclear multidimensional NMR spectroscopy as described previously (*21*). In general, pulsed field gradients were typically included to purge undesired transverse magnetization (*23*), and the WATERGATE technique was used in most cases to suppress the solvent signal in samples dissolved in H_2O. In samples dissolved in D_2O, presaturation of the HDO resonance was used. The backbone coupling constants ($^3J_{NH-H\alpha}$) of S100A1 were measured using the HNHA experiment and evaluated as described previously (*24*). Data were processed on Silicon Graphics workstations with the software package NMRPIPE (*25*). All proton chemical shifts are reported with respect to the H_2O or HDO signal, which is taken as 4.658 ppm downfield from external TSP (0.0 ppm) at 37 °C. The ^{13}C and ^{15}N chemical shifts were indirectly referenced using the following ratios of the zero-point frequencies at 37 °C: 0.10132905 for ^{15}N to ^1H and 0.25144953 for ^{13}C to ^1H as previously described (*26*−*28*). These ^1H, ^{13}C, and ^{15}N chemical shift values were deposited previously in the BioMagResBank database (accession number: 4285).

Structure Calculations. Strong, medium, and weak NOE correlations assigned in 2D, 3D, and 4D NOESY experiments were included as interproton distance constraints in structure calculations as previously described (*29*). Dihedral constraints $\phi \pm 20°$ and $\psi \pm 15°$ for α-helix and $\phi \pm 40°$ and $\psi \pm 40°$ for β-sheet were included on the basis of $^3J_{NH-H\alpha}$ coupling constants, hydrogen exchange rates, and chemical shift index of $^1H^\alpha$ and $^{13}C^\alpha$ (*30*). Hydrogen bond constraints of $r_{NH-O} = 1.5-2.8$ Å and $r_{N-O} = 2.4-3.5$ Å were included in the final stage of structure calculations. One hundred and fifty structures were calculated with the computer program X-PLOR version 3.851 (*31*) using a $(\sum r^{-6})^{-1/6}$ sum for the distance-dependent constraints. Standard protocols for substructure embedding, regularization, hybrid distance geometry-simulated annealing (DGSA) regularization/refinement, and simulated annealing (SA) were used in these calculations. To retain symmetry in the S100A1 homodimer, the DGSA and SA routines contained noncrystallographic symmetry (NCS) and distance symmetry constraints with force constants of 100 and 1 kcal mol^{-1} Å^{-2}, respectively (*32*). Pseudopotentials for secondary $^{13}C_\alpha$ and $^{13}C_\beta$ chemical shifts and a conformational database potential were included in the final SA refinement (*33*). When hydrogen bond restraints and the conformational database potential were omitted, however, no change in the structure within the RMSD of the acceptable structures was observed. This refinement procedure yielded several structures (>70) with zero NOE violations >0.2 Å and no dihedral violations >5° consistent with all of the NMR data. The final 20 structures were chosen on the basis of their lowest energy. The statistics for the family of low-energy structures are listed in Table 1, and their coordinates are in the Protein Data Bank (PDB) with the accession number 1K2H (RCSB 014477).

Structure Calculation for the S100A1/B Heterodimer. To model the S100A1/B heterodimer, individual subunits from each of the lowest energy structures of S100B (*34*) and S100A1 were manually docked together. This docking was based on core-forming dimer interactions found in each of the homodimeric structures. While the manually docked model had little van der Waals overlap, it was subjected to energy minimization nevertheless. This was done using 400 steps of steep descent energy minimization with the computer program CHARMm (Harvard University) and an adopted basis Newton−Raphson method (ABNR). The final energy-minimized structure successfully eliminated all van der Waals contacts and retained ideal bond lengths, angles, and planarities.

Table 1: NMR Constraints and Statistics of 20 NMR Structures[a]

	⟨20⟩	best
rmsds from distance constraints (Å)[b]		
total (2410)	0.0497 ± 0.0013	0.048
intraresidue (498)	0.0039 ± 0.0025	0.009
sequential ($\|i-j\|=1$) (688)	0.0342 ± 0.0034	0.030
medium range ($1<\|i-j\|\le 1$) (682)	0.0608 ± 0.0026	0.060
long range ($\|i-j\|>5$) (272)	0.0738 ± 0.0065	0.070
intermolecular for dimer interface (80)	0.0574 ± 0.0112	0.059
intra- and/or intermolecular (22)	0.0194 ± 0.0165	0.016
hydrogen bonds (168)	0.0705 ± 0.0057	0.066
rmsds from exptl dihedral constraints[b]		
ϕ, ψ (258)	0.613 ± 0.122	0.442
rmsds from exptl ^{13}C chemical shifts		
$^{13}C_\alpha$ (ppm)	1.278 ± 0.080	1.227
$^{13}C_\beta$ (ppm)	1.058 ± 0.108	1.058
rmsds from idealized covalent geometry		
bonds (Å)	0.0063 ± 0.0002	0.0063
angles (deg)	0.806 ± 0.0169	0.796
impropers (deg)	1.895 ± 0.0076	1.890
Lennard-Jones potential energy (kcal/mol)[c]	−753 ± 29	−776
% of residues in most favorable region[d]	84.2 ± 1.8	86.2
rmsds to mean structure (Å)[e]		
all ordered backbone in S100A1 (2−88)	0.65 ± 0.08	0.67
all ordered heavy atoms in S100A1 (2−88)	1.26 ± 0.10	1.28
all backbone in S100A1 (1−93)	1.00 ± 0.31	1.06
all heavy atoms in S100A1 (1−93)	1.60 ± 0.27	1.72

[a] The 20 ensemble structures were obtained from simulated annealing (SA) calculations. The best structure is chosen from the lowest total energy. For ⟨20⟩, the values shown are the mean ± standard deviation. The force constants used in the SA calculations are as follows: 1000 kcal mol^{-1} Å^{-2} for bond length, 500 kcal mol^{-1} rad^{-2} for angles and improper torsions, 4 kcal mol^{-1} Å^{-4} for the quartic van der Waals (vdw) repulsion term (hard-sphere effective vdw radii set to 0.8 times their values in the CHARMm parameters), 50 kcal mol^{-1} Å^{-2} for experimental distance constraints, 150 kcal mol^{-1} rad^{-2} for dihedral constraints, 100 kcal mol^{-1} Å^{-2} for noncrystallographic symmetry, 1 kcal mol^{-1} Å^{-2} for distance symmetry constraints, 0.5 kcal mol^{-1} ppm^{-2} for ^{13}C chemical shift constraints, and 1.0 for conformational database potential. [b] None of the 20 structures has a distance violation of >0.4 Å or a dihedral angle violation of >5°. [c] Lennard-Jones van der Waals energy was calculated using the CHARMm parameters and was not employed in any stage of structure calculations. [d] PROCHECK was employed to obtain the Ramachandran plot and other parameters. [e] Ordered backbone calculations included C_α, N, and C′ atoms. Only residues 2−88 in the S100A1 protein are included since no medium- to long-range NOE correlations were observed for residues 1 and 89−93.

RESULTS AND DISCUSSION

Three-Dimensional Structure of S100A1. A total of 498 intraresidue, 688 sequential, 682 medium-range, 272 long-range, and 80 intermolecular NOE correlations were assigned using the complete sequence-specific resonance assignments

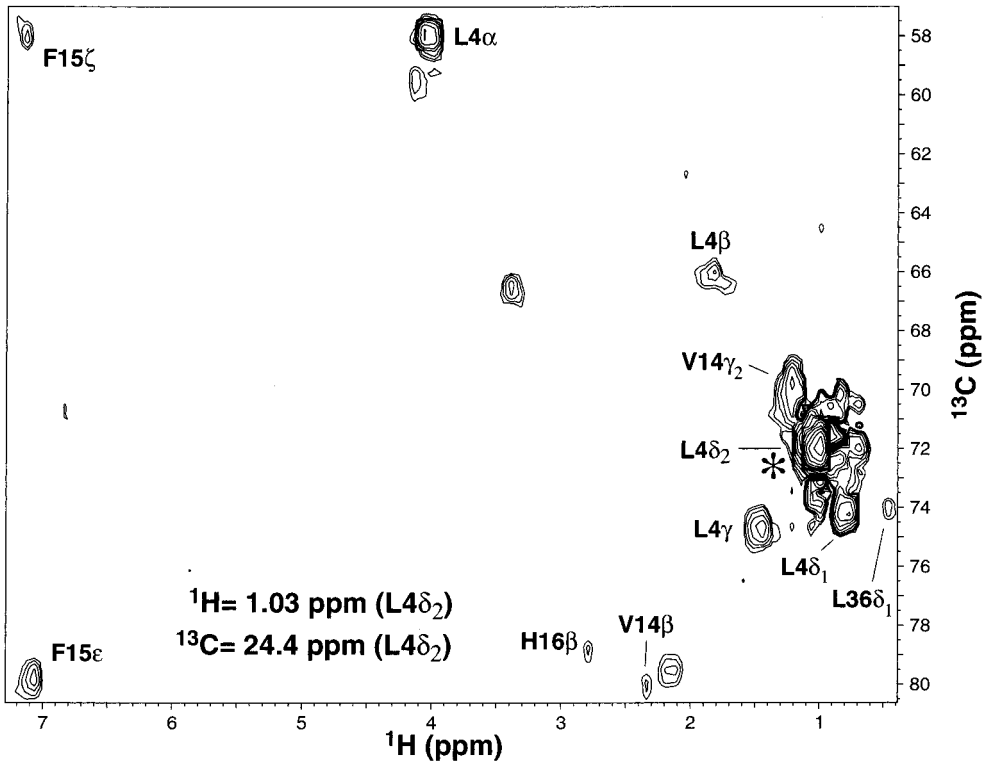

FIGURE 1: NOE spectrum illustrating intermolecular correlations at the dimer interface. A plane from a 4D $^{13}C,^{13}C$-edited NOESY spectrum shows intermolecular NOE correlations from L4δ_2 (in helix 1) in the dimer interface to V14, F15, and H16 (helix 1′) and L36 (helix 2′) of S100A1. NOE correlations marked with asterisks are autocorrelations. NOE correlations not labeled have their maximal intensity in different planes.

for the backbone and side chain ^1H, ^{13}C, and ^{15}N resonances of S100A1 reported previously (*21*). In addition, all of the NOE correlations used as distance constraints in the structure calculation were checked for their reciprocal NOE correlation. In many cases, however, a significant number of degeneracies in chemical shift were noted during the assignment of NOE correlations, probably due to the presence of four α-helices in each subunit of S100A1 and because of degeneracies resulting from the symmetric dimer interface. As a result, the assignment of NOE correlations from 2D and 3D NOESY data sets alone was difficult. Thus, 4D $^{13}C,^{15}N$-edited NOESY and $^{13}C,^{13}C$-edited NOESY experiments were used routinely to resolve these ambiguities. With these 4D data, over 50% of the long-range and intermolecular NOE correlations were assigned, based solely on unambiguous chemical shift values (Figures 1 and 2). Additional NOE correlations were added iteratively using preliminary structural models of S100A1.

At an early stage in the NOE assignment process, it was found that helices 1 and 4 were an integral part of the S100A1 dimer interface as found previously for apo-S100B and apo-S100A6 (*34*, *35*). For example, an unambiguous intermolecular NOE assignment was made between the H_δ protons of L4 in helix 1 and protons of V14, F15, and H16 in helix 1′ (Figure 1). The distance constraint between the protons of these residues was assigned as intermolecular because of the physical impossibility of having the N- and C-terminus of helix 1 being close together in space. Likewise, several intermolecular NOE correlations between protons from the N- and C-terminus of helix 4 were assigned, indicating that helices 4 and 4′ align in an antiparallel manner at the dimer interface. These and other unambiguous intermolecular NOE assignments made it possible to assign a large number of intersubunit NOE correlations. Intermolecular NOE correlations, which could not be assigned using chemical shift values alone, were assigned on the basis of structural considerations and included at later stages in the refinement process. An additional 20 NOE correlations remained ambiguous (Table 1), and they were allowed to satisfy inter- and/or intramolecular distance constraints as previously described for other symmetric dimers (*32*). However, the omission of these 20 ambiguous constraints did not affect the tertiary fold of the S100A1 dimer (rmsd < 0.6 Å). In total, the dimer interface of S100A1 was defined by 80 unambiguous intermolecular NOE connectivities between residues in helix 1 (E3, L4, E5, A7, M8, L11, I12, V14, F15, H16, H18), loop 2 (E40, L41), helix 4 (V69, F71, Q72, V76, L77, V78, A79, A80, T82, V83), and loop 4 (N86, F88). Several of these residues, at the core of the S100A1 dimer interface, are homologous to residues that give rise to intermolecular NOE correlations in the S100B dimer (helix 1, E2, L3, E4, A6, M7, V8, A9, L10, I11, V13, F14, and Y17; helix 2, L35, I36, N37, E39, L40, and S41; loop 2, F43; helix 3, V52; helix 4, F70, Q71, M74, A75, F77, M79, T81, and T82; and loop 4, F87 and F88).

Calculations of the S100A1 solution structure included a total of 2410 intra- and intermolecular NOE correlations, dihedral angle correlations, and NMR-based hydrogen bond constraints (over 13.1 constraints/residue; Table 1). Figure 3 illustrates the superposition of the 20 lowest energy structures that best fit the input data. None of these structures contained NOE violations exceeding 0.4 Å, dihedral angle violations exceeding 5°, or hydrogen bond violations (Table 1). Furthermore, these 20 structures were found to have a

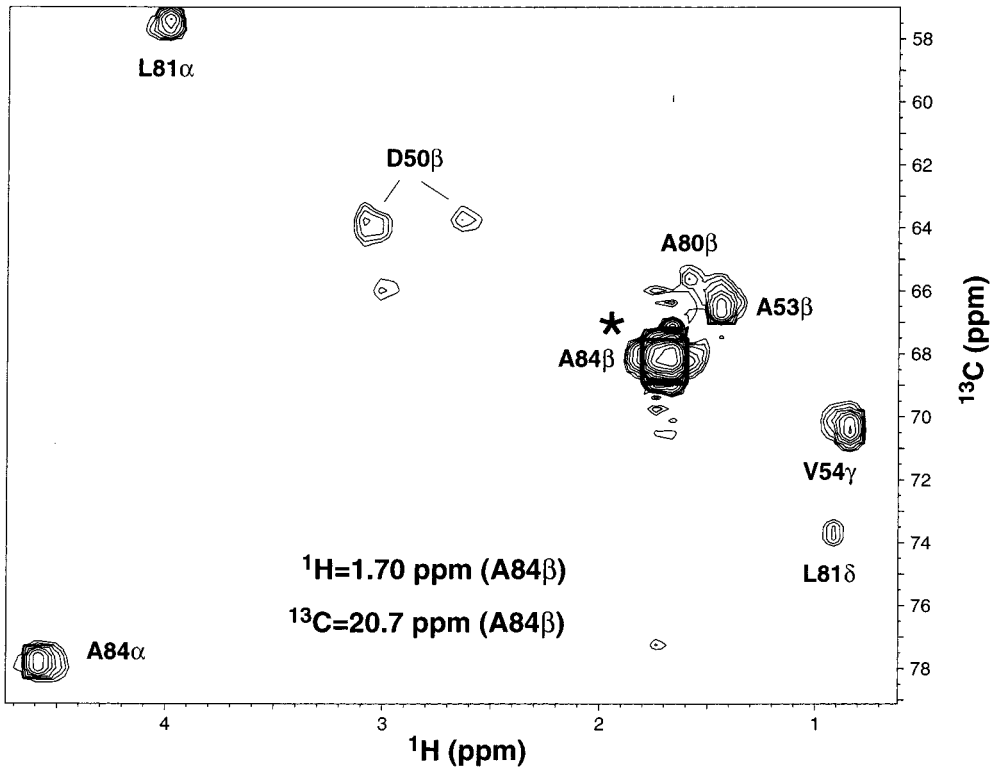

FIGURE 2: Plane from a 4D ^{13}C,^{13}C-edited NOESY spectrum illustrating long-range intramolecular NOE correlations for residue A84 in helix 4 to residues D50, A53, and V54 in helix 3. This plane also shows an *i*, *i* + 3 NOE correlation for L81α to A84*β*. NOE correlations marked with asterisks are autocorrelations, and those correlations not labeled have their maximal intensity in different planes.

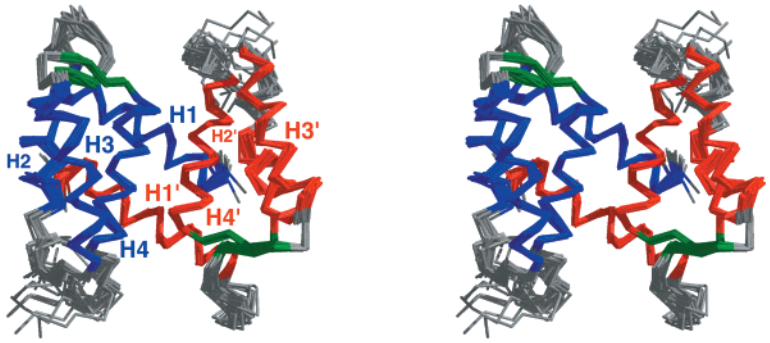

FIGURE 3: Overlay of 20 low-energy structures of S100A1 based on NMR-derived constraints. The helices for each subunit are shown in different colors (red and blue), and the *β*-strands are shown in green for both subunits. The statistics for this family of structures are given in Table 1.

low root mean square difference (rmsd) when calculated from the average structure (<0.65 Å for backbone atoms; <1.26 Å for all atoms; Table 1). The best of these structures (Figure 4) was chosen because of its lowest deviation from idealized geometry as judged by minimal deviations from idealized bond lengths and dihedral angles and based on the minimal number of van der Waals contacts (Table 1). The Ramachandran diagram of the best-fit dimer structure shows that no residues are outside of the allowed range of the backbone angles phi and psi (ϕ, ψ) with a majority of the residues being in the most favored region of the diagram (86%; Table 1). Finally, the overall stereochemical quality of the set of structures shown in Figure 3, assessed by several programs of PROCHECK (*36*), indicates that the S100A1 dimer structure is comparable to that of a 2 Å well-defined X-ray structure with an *R* factor <20%.

Each subunit of dimeric S100A1 contains two helix−loop−helix Ca^{2+}-binding domains known as EF-hands. Together, the four helices in each subunit adopt a three-dimensional fold resembling a unicornate-type four-helical bundle (*37*). The two Ca^{2+}-binding domains of each S100α subunit contain a short *β*-strand segment, K27−S29 (strand 1) and G67−D70 (strand 2), respectively, which aligns in an antiparallel manner. This small *β*-sheet brings the two helix−loop−helix domains into close proximity in a manner similar to other EF-hand containing proteins (*38*) including those in the S100 protein family (*11*).

Helix 1 is the first helix in the pseudo-EF-hand domain of S100A1, and residues E3 through A17 of helix 1 all have ϕ and ψ backbone dihedral angles typical of an α-helix. Although many of the residues in helix 1 are involved in the dimer interface, a large number of intrasubunit interactions are also observed. For example, several residues from the C-terminus of helix 1 interact with the first Ca^{2+}-binding loop (loop 1) and helix 2 in a manner similar to other members of the EF-hand superfamily. Thus, helices 1 and 2

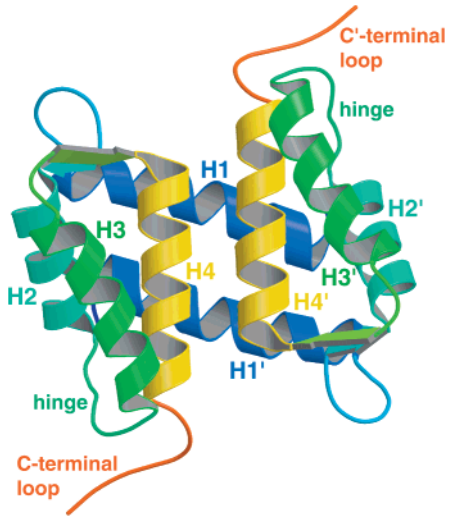

FIGURE 4: Ribbon diagram of the lowest energy structure of S100A1. The helices in each subunit of S100A1 are shown in different colors.

in the first helix−loop−helix Ca^{2+}-binding domain of apo-S100A1 align with an interhelical angle of 120°, which is similar to that observed for apo-S100B (133°) and apocalcyclin (126°), respectively (Table 2). Interestingly, in the absence of Ca^{2+} it is found that the two helices of EF-hands in apocalmodulin and apocalbindin align (∼140°) to maximize energetically favorable interhelical interactions and that a nearly perpendicular alignment of the two helices is usually a signature for the Ca^{2+}-bound state (*38*). This suggests that a realignment of helices 1 and 2 in S100A1 upon binding Ca^{2+} may be a small feature of its conformational change. This feature would be similar to other S100 proteins such as S100B and S100A6, in which this interhelical angle between helices 1 and 2 does not change appreciably upon the addition of divalent metal (*34*, *35*, *39*−*42*). As with other S100 proteins, the significant involvement of helix 1 at the dimer interface in the apo state is another reason the potential realignment of helices 1 and 2 upon binding Ca^{2+} is unlikely.

The second helix−loop−helix Ca^{2+} ion-binding domain of S100A1 consists of helix 3, loop 3, and helix 4. The N-terminal residues of helix 3 are found to interact with the C-terminal residues of helix 4 as defined by a large number of unambiguous NOE correlations (Figure 2) observed between residues D50, A53, and V54 (in helix 3) and residues A80, L81, V83, and A84 (in helix 4). The orientation of helix 3 was further defined by a large number of unambiguous long-range NOE correlations between the C-terminus of helix 3 to the N-terminus of helix 2 including those from residues M58, E60, and L61 to residues K30, K31, and K34. The resulting interhelical angle (−150° or 210°) between helices 3 and 4 is quite unlike the alignment in the pseudo-EF-hand of S100A1 (where it is 120°) but more similar to the helix 3/4 angle found in another S100 protein, S100B (−166°). Consequently, the helices in this EF-hand of S100A1 will have to reorient by at least 90° upon binding Ca^{2+} in order to obtain a conformation typical of any other EF-hand containing protein in the Ca^{2+}-bound state (∼100 ± 15°). This potentially large change in protein conformation would certainly explain the large changes that were observed in NMR and fluorescence spectra upon the addition of a single equivalent of Ca^{2+} (data not shown) as well as explain the Ca^{2+} dependence observed for binding several target proteins (*12*, *43*).

Two loops of S100A1 (loops 2 and 4) have the least amount of sequence homology to other S100 proteins, and these loops are important for binding effector proteins (*11*, *12*, *44*). In apo-S100A1, the hinge (loop 2) and C-terminal loop (loop 4) are proximal in space (Figure 4), and together they form a surface including the C-terminal regions of helices 2 and 4 and the N-terminal region of helix 3. A similar orientation of these analogous loops is also found in apo-S100B (*34*). Therefore, on the basis of the large reorientation of these loops observed when the apo-S100B and Ca^{2+}-bound S100B structures are compared, it is also likely that these two loops in S100A1 will separate upon the addition of Ca^{2+} to allow for target protein binding.

Several of the highly conserved hydrophobic residues within the S100 protein family are involved in the dimer interface of S100A1 as previously observed in the high-resolution structures of apo-S100B and apo-S100A6 (*34*, *35*). These include residues L4, A7, M8, T10, L11, I12, V14, F15, H16, H18, F71, Q72, V75, V78, A79, T82, V83, and F88. In S100A1, the majority of the dimer interface is defined by the nearly antiparallel alignment of helices 1 and 1′ (−165°) and helices 4 and 4′ (176°), respectively (Figure 5). The antiparallel orientation of these helices is similar to

Table 2: Interhelical Angles of S100 Proteins and Protein Complexes[a]

helices	apo-S100A1[b]	apo-S100B[b,c]	apo-S100A6[b,d]	NMR Ca^{2+}-S100B[b,e]	X-ray Ca^{2+}-S100B[b,f]	S100B−Ca^{2+}−p53[b,g]
I−II	$120 \pm 3^{\perp}$	$133 \pm 1^{\perp}$	$126 \pm 2^{\perp}$	$137 \pm 5^{\perp}$	$137^{\perp}$	$120 \pm 3^{\perp}$
I−III	$-45 \pm 2^{\perp}$	$-46 \pm 1^{\perp}$	$-52 \pm 2^{\perp}$	$-118 \pm 5^{\perp}$	$-120^{\perp}$	$-123 \pm 2^{\perp}$
I−IV	$107 \pm 2^{\perp}$	$120 \pm 1^{\perp}$	$115 \pm 1^{\perp}$	$128 \pm 4^{\perp}$	$129^{\perp}$	$125 \pm 1^{\perp}$
II−III	$148 \pm 2^{\parallel}$	$149 \pm 1^{\parallel}$	$-164 \pm 2^{\parallel}$	$104 \pm 3^{\perp}$	$102^{\perp}$	$115 \pm 2^{\perp}$
II−IV	$-46 \pm 1^{\parallel}$	$-40 \pm 1^{\parallel}$	$-45 \pm 1^{\perp}$	$-35 \pm 4^{\parallel}$	$-30^{\parallel}$	$-26 \pm 2^{\parallel}$
III−IV	$-150 \pm 1^{\parallel}$	$-166 \pm 1^{\parallel}$	$150 \pm 2^{\parallel}$	$106 \pm 4^{\perp}$	$105^{\perp}$	$110 \pm 1^{\perp}$
I−I′	$-165 \pm 3^{\parallel}$	$-153 \pm 1^{\parallel}$	$-144 \pm 1^{\parallel}$	$-155 \pm 1^{\parallel}$		$-152 \pm 2^{\parallel}$
I−IV′	$-72 \pm 3^{\perp}$	$-66 \pm 1^{\perp}$	$-76 \pm 1^{\perp}$	$-58 \pm 3^{\perp}$		$-66 \pm 1^{\perp}$
IV−IV′	$176 \pm 2^{\parallel}$	$155 \pm 1^{\parallel}$	$148 \pm 1^{\parallel}$	$159 \pm 5^{\parallel}$		$138 \pm 2^{\perp}$

[a] Interhelical angles (Ω) range from −180° to +180° and are classified as either parallel (∥) for 0° ≤ |Ω| ≤ 40° and 140° ≤ |Ω|≤ 180° or as perpendicular (⊥) for 40° < |Ω| < 140° as described (*37*). [b] Interhelical angles were calculated using the computer programs Iha 1.4 and Interhlx. [c] Taken from the NMR structure (PDB code 1B4C) of Drohat et al. (*34*). Two other lower resolution structures of apo-S100B are also available [PDB codes 1SYM and 1CFP (*39*, *45*)]. [d] Taken from the NMR structure (PDB code 2CNP) of Mäler et al. (*35*). [e] Taken from the NMR structure (PDB code 1QLK) of Drohat et al. (*40*). Another NMR structure (PDB code 1UWO) reported by Smith and Shaw (*46*) is also in good agreement with the NMR and X-ray structures for Ca^{2+}-loaded S100B($\beta\beta$) in this table. [f] Taken from the X-ray crystal structure (PDB code 1MHO) of Matsumura et al. (*42*). [g] Taken from the NMR structure (PDB code 1DT7) of Rustandi et al. (*44*). The interhelical angles from the p53 peptide to helices I−IV are 139 ± 3 (I), 100 ± 3 (II), −16 ± 3 (III), and 95 ± 3 (IV), respectively.

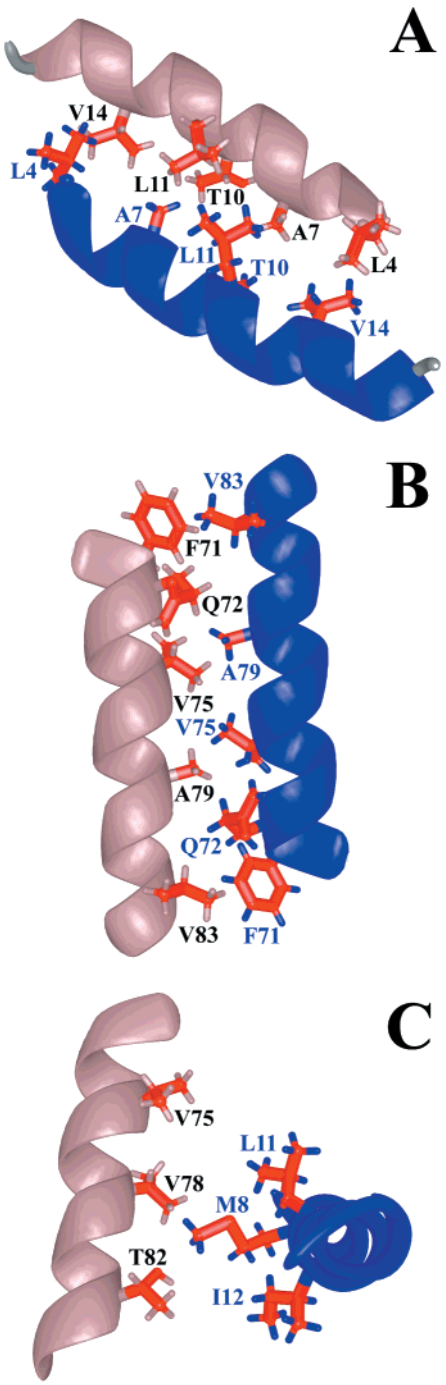

FIGURE 5: Dimer interface of S100A1. Shown in (A) are the residues involved in the helix 1/helix 1′ interface. (B) Residues in the helix 4/helix 4′ interface and (C) residues in the helix 1/helix 4′ interface are also illustrated.

that observed for S100B and S100A6, where helices 4 and 4′ at the dimer interface align in an antiparallel manner with an angle of 155° and 148°, respectively (Table 2). In addition, helices 1 and 1′ of S100A1 are nearly perpendicular to helices 4 and 4′, respectively, to give an X-type four-helical bundle as found for several proteins in the S100 family (Figures 4 and 5). The stability of the S100A1 dimer is further evident from the fact that several hydrophobic amino acid residues from each subunit of S100A1 are arranged to form a distinct hydrophobic core that extends through the dimer interface (Figure 5). The highly favorable distribution of charged residues on the surface and hydrophobic residues buried in

Table 3: Comparison of Residues at the Dimer Interface of S100A1, S100B, and S100A6 to Monomeric Calbindin D_{9K}

helix 1−1′ interactions[a]	position[b] 4	7	10	11	14
S100A1	L	A	T	L	V
S100B	L	A	*A*[c]	L	V
S100A6	L	A	*L*	L	*I*
calbindin D_{9K}	*A*	*S*	E[d]	L	*I*

helix 4−4′ interactions	position[a] 71	72	75	79	83
S100A1	F	Q	V	A	V
S100B	F	Q	*M*	A[e]	*T*
S100A6	F	Q	V	*G*	*L*
calbindin D_{9K}	F	E	*Q*	K	*Q*

helix 1−4′ interactions	position[a] 8	11	12	75	78	82
S100A1	M	L	I	V	V	T
S100B	M	L	I	*M*	V	T
S100A6	*I*	L	*V*	V	*L*	*A*
calbindin D_{9K}	*P*	L	K	*Q*	V	*S*

[a] Helix−helix interactions at the dimer interface of S100A1, S100B, and S100A6. Calbindin D_{9K} does not form a homodimer in solution, but it is listed here for comparison. [b] Sequences are aligned using the residue numbering of S100A1. [c] Shown in *italics* are residues that are not identical to S100A1 at that sequence position. [d] Underlined residues represent charged residues that likely contribute to calbindin D_{9K} existing as a monomer in solution. [e] This residue is a serine in rat S100B and an alanine in human S100B.

the core of S100A1 is now typical for most S100 proteins and can explain why this protein family is so highly soluble even in the absence of Ca^{2+}.

Model of the S100A1/B Heterodimer. Because the dimer interface of S100A1 is very similar to that of S100B (Table 3), it was possible to model the S100A1/B heterodimer. For example, 13 of the 16 residues are identical between S100B and S100A1 at the innermost core of the dimer interfaces. These include residues L4, A7, L11, and V14 at the helix 1/helix 1′ interface (Figure 5A), residues F71, Q72, and V75 at the helix 4/helix 4′ interface (Figure 5B), and residues M8, L11, I12, V78, A79, and T82 at the helix 1/helix 4′ interface (Figure 5C). The three remaining residues are conservative changes when the two proteins are compared (helix1/helix 1′ interface, T10A; helix 4/helix 4′ interface, A79S, V83T; helix 4/helix 1′ interface; V75M; Table 3). Because of the striking similarity between these two proteins, the dimer interface of apo-S100B, apo-S100A1, and the model of the S100A1/B heterodimer are packed in a nearly identical manner (Figure 6). Only a very slight change in side chain positioning occurs in the helix 1/helix 4′ interface because of the difference at position 75 (V75M; Table 3), but this very slight difference has no effect on the backbone or on the overall global fold on either of the dimers.

The model for the heterodimer (Figure 5) is supported by comparisons of chemical shift assignments of S100B in the S100A1/B heterodimer to that of S100B in the homodimer. This was done by titrating unlabeled S100A1 into ^{15}N-labeled S100B (rat) and monitoring the changes in intensity and chemical shift of the S100B resonances. When these chemical shifts are compared, differences in proton and/or ^{15}N chemical shift (>0.1 ppm) were observed for residues in helix 1 (L3, K5, and D12), the pseudo-EF-hand (G19, D23,

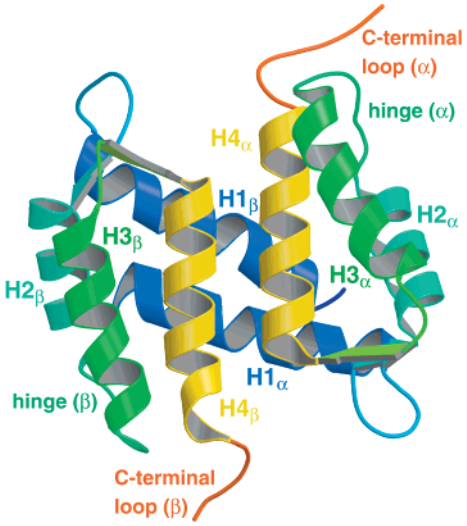

FIGURE 6: Ribbon diagram of a model for the S100A1/B heterodimer.

K26, and K28), helix 2 (E34), the typical EF-hand (G64), and helix 4 (D69, F71, A75, F76, V80, and A83) of S100B. These chemical shift changes indicate that a subunit of unlabeled S100A1 displaces a subunit of S100B to form the heterodimer (Figure 5). Consistent with the heterodimer model (Figure 5), no chemical shift perturbations were observed for residues in helix 3 because of their relatively large distance from the dimer interface. The changes in chemical shift for residues in helix 1 can be explained by variations in sequence between S100B and S100A1 at the core of the helix 1/helix 1′ dimer interface (Table 3). At position 10, S100A1 has a threonine residue, whereas an alanine residue is at the analogous position for S100B (A9). Likewise, the chemical shift changes for residues in helix 4 can be explained by differences in the proteins' sequences at positions 83 (V83T; using the S100A1 numbering), 79 (A79S), and 75 (V75M) and considering the antiparallel alignment of helices 4 and 4′ as predicted by the model (Figure 5; Table 3). The chemical shift changes observed in the EF-hand domains are generally smaller and may result from slight differences in the orientation of the helices comprising the helix−loop−helix calcium-binding domains, but this phenomenon needs yet to be confirmed with a more rigorous structural characterization of the heterodimer.

Why Is Calbindin D_{9K} the Only Monomeric S100 Family Member? Calbindin D_{9K} is the one S100 protein family member that does not form a homodimer, and it does not form heterodimers with other S100 proteins. When the sequence of calbindin D_{9K} is aligned with the sequences of S100A1, S100A6, and S100B, there are very striking differences at several positions (Table 3). The most notable amino acid residue changes are the presence of charged residues in calbindin D_{9K} that would be in the hydrophobic core at four positions (T10E, Q72E, A79K, I12K) of either S100A1, S100A6, or S100B (Table 3). In addition, eight other amino acid differences occur when the sequence of calbindin D_{9K} is compared to residues that make up the core of S100A1, S100A6, and S100B dimer interfaces. Thus, it is not surprising that calbindin D_{9K} does not form dimers since a large number of its residues are different from those in the core of the dimer interface for S100A1, S100B, and S100A6.

Summary. The three-dimensional solution structure of apo-S100A1 was determined in solution using multidimensional heteronuclear NMR techniques. The structure of apo-S100A1 indicates that the dimer interface of this Ca^{2+}-binding protein is held together noncovalently to form an X-type four-helix bundle at the dimer interface much like that of other members of this protein family. The only S100 protein that does not form dimers, calbindin D_{9K}, has several charged residues located in what is the dimer core of S100A1. Because the 16 residues that form the inner core of the dimer of the S100A1 and S100B dimers are 100% homologous (75% identical), it was possible to model the S100A1/B heterodimer. Not surprisingly, it was found that the model for the S100A1/B heterodimer has a 3D structure much like each of the individual homodimers.

The conformational change in S100A1 likely involves the reorientation of helix 3 by more than 90°. This change in conformation would be necessary for apo-S100A1 to acquire the three-dimensional shape of other well-characterized EF-hand proteins in the presence of Ca^{2+}. As for most S100 proteins, this conformational change can explain why there is a Ca^{2+} dependence for S100A1 binding to most of its protein targets.

SUPPORTING INFORMATION AVAILABLE

One table giving parameters for NMR experinents. This material is available free of charge via the Internet at http://pubs.acs.org.

REFERENCES

1. Donato, R. (1991) *Cell Calcium 12*, 713−726.
2. Donato, R. (1999) *Biochim. Biophys. Acta 1450*, 191−231.
3. Zimmer, D. B., and Landar, A. (1995) *J. Neurochem. 64*, 2727−2736.
4. Schäfer, B. W., and Heizmann, C. W. (1996) *Trends Biochem. Sci. 21*, 134−140.
5. Zimmer, D. B., Cornwall, E. H., Landar, A., and Song, W. (1995) *Brain Res. Bull. 37*, 417−429.
6. South, A. P., Cabral, A., Ives, J. H., James, C. H., Mirza, G., Marenholz, I., D., M., Backendorf, C., Ragoussis, J., and Nizetic, D., N. (1999) *J. Invest. Dermatol. 112*, 910−918.
7. Zimmer, D. B., Cornwall, E. H., Reynolds, P. D., and Donald, C. M. (1998) *J. Biol. Chem. 273*, 4705−4711.
8. Baudier, J., Glasser, N., and Gerard, D. (1986) *J. Biol. Chem. 261*, 8192−8203.
9. Baudier, J., and Gerard, D. (1986) *J. Biol. Chem. 261*, 8204−8212.
10. Kligman, D., and Hilt, D. (1988) *Trends Biochem. Sci. 13*, 437−443.
11. Weber, D. J., Rustandi, R. R., Carrier, F., and Zimmer, D. B. (2000) *Interaction of dimeric S100B(ββ) with the tumor suppressor protein: A model for Ca-dependent S100-target protein interactions*, Kluwer Academic Publishers, Dordrecht, The Netherlands.
12. Landar, A., Rustandi, R. R., Weber, D. J., and Zimmer, D. B. (1998) *Biochemistry 37*, 17429−17438.
13. Osterloh, D., Ivanenkov, V. V., and Gerke, V. (1998) *Cell Calcium 24*, 137−151.
14. Harrison, C. A., and Geczy, C. L. (1999) *J. Biol. Chem. 274*, 8561−8569.
15. Drohat, A. C., Nenortas, E., Beckett, D., and Weber, D. J. (1997) *Protein Sci. 6*, 1577−1582.
16. Bhardwaj, R. S., Zotz, C., Swaldoklarwasser, G., Roth, J., Goebeler, M., Mahnke, K., Falk, M., Meinards-Hager, G., and Sorg, C. (1992) *Eur. J. Immunol. 22*, 1891−1897.

17. Teigelkamp, S., Bhardwaj, R. S., Roth, J., Meinards-Hager, G., Karas, M., and Sorg, C. (1991) *J. Biol. Chem. 266*, 13462−13467.
18. Kato, K., and Kimura, S. (1985) *Biochim. Biophys. Acta 842*, 146−150.
19. Wang, G., Rudland, P. S., White, M. R., and Barraclough, R. (2000) *J. Biol. Chem. 275*, 11141−11146.
20. Tarabykina, S., Kriajevska, M., Scott, D. J., Hill, T. J., Lafitte, D., Derrick, P. J., Dodson, G. G., Lukanidin, E., and Bronstein, I. (2000) *FEBS Lett. 475*, 187−191.
21. Baldisseri, D. M., Rustandi, R. R., Zhang, Z., Tang, C., Bair, C. L., Landar, A., Landar, A., Zimmer, D. B., and Weber, D. J. (1999) *J. Biomol. NMR 14*, 91−92.
22. Marion, D., Ikura, M., Tschudin, R., and Bax, A. (1989) *J. Magn. Reson. 85*, 393−399.
23. Bax, A., and Pochapsky, S. S. (1992) *J. Magn. Reson. 99*, 638−643.
24. Vuister, G. W., and Bax, A. (1992) *J. Biomol. NMR 2*, 401−405.
25. Delaglio, F., Grzesiek, S., Vuister, G. W., Zhu, G., Pfeifer, J., and Bax, A. (1995) *J. Biomol. NMR 6*, 277−293.
26. Spera, S., and Bax, A. (1991) *J. Am. Chem. Soc. 113*, 5490−5492.
27. Live, D. H., Davis, D. G., Agosta, W. C., and Cowburn, D. (1984) *J. Am. Chem. Soc. 106*, 1939−1941.
28. Edison, A. S., Abilgaard, F., Westler, W. M., Mooberry, E. S., and Markley, J. L. (1994) *Methods Enzymol. 239*, 3−79.
29. Clore, G. M., Nilges, M., Sukumaran, D. K., Brunger, A. T., Karplus, M., and Gronenborn, A. M. (1986) *EMBO J. 5*, 2729−2735.
30. Wishart, D. S., and Sykes, B. D. (1994) *J. Biomol. NMR 4*, 171−180.
31. Brunger, A. T. (1992) *X-PLOR Version 3.1, A system for X-ray crystallography and NMR*, Yale University, New Haven, CT.
32. Nilges, M. (1993) *Proteins: Struct., Funct., Genet. 17*, 297−309.
33. Kuszewski, J., Gronenborn, A. M., and Clore, G. M. (1997) *J. Magn. Reson. 125*, 171−177.
34. Drohat, A. C., Tjandra, N., Baldisseri, D. M., and Weber, D. J. (1999) *Protein Sci. 8*, 800−809.
35. Maler, L., Potts, B. C. M., and Chazin, W. J. (1999) *J. Biomol. NMR 13*, 233−247.
36. Laskowski, R. A., MacArthur, M. W., Moss, D. S., and Thornton, J. M. (1993) *J. Appl. Crystallogr. 26*, 283−291.
37. Harris, N. L., Resnell, S. R., and Cohen, F. E. (1994) *J. Mol. Biol. 236*, 1356−1368.
38. Strynadka, N. C. J., and James, M. N. G. (1989) *Annu. Rev. Biochem. 58*, 951−998.
39. Drohat, A. C., Amburgey, J. C., Abildgaard, F., Starich, M. R., Baldisseri, D., and Weber, D. J. (1996) *Biochemistry 35*, 11577−11588.
40. Drohat, A. C., Baldisseri, D. M., Rustandi, R. R., and Weber, D. J. (1998) *Biochemistry 37*, 2729−2740.
41. Sastry, M., Ketchem, R. R., Crescenzi, O., Weber, C., Lubienski, M. J., Hidaka, H., and Chazin, W. J. (1998) *Structure 6*, 223−231.
42. Matsumura, H., Shiba, T., Inoue, T., Harada, S., Kai, Y. (1998) *Structure 6*, 233−241.
43. Garbuglia, M., Verzini, M., Rustandi, R. R., Osterloh, D., Weber, D. J., Gerke, V., and Donato, R. (1999) *Biochem. Biophys. Res. Commun. 254*, 36−41.
44. Rustandi, R. R., Baldisseri, D. M. Weber, D. J. (2000) *Nat. Struct.Biol. 7*, 570−574.
45. Kilby, P. M., Van Eldik, L. J., and Roberts, G. C. K. (1996) *Structure 4*, 1041−1052.
46. Smith, S. P., and Shaw, G. S. (1998) *Structure 6*, 211−222.

BI0118308